nature geoscience

Article

https://doi.org/10.1038/s41561-023-01193-4

Late Miocene onset of hyper-aridity in East Antarctica indicated by meteoric beryllium-10 in permafrost

Received: 16 September 2021

Accepted: 26 April 2023

Published online: 29 May 2023

Check for updates

Marjolaine Verret[1,2] ✉, Cassandra Trinh-Le[3], Warren Dickinson[1], Kevin Norton[3], Denis Lacelle[4], Marcus Christl[5], Richard Levy[1,6] & Tim Naish[1]

Continental-scale ice sheets have covered Antarctica since an interval of global cooling near the Eocene–Oligocene boundary around 33.9 million years ago (Ma). However, the sequence of events that led to the emergence of the persistent ice sheet in modern East Antarctica remains disputed. The transition to permanent polar aridity in high elevations of East Antarctica is critical to our understanding of the threshold response of glacial systems in Antarctica to changes in surface temperature at lower elevations. Here we constrain the onset of the polar aridity—which was probably necessary for regional ice-sheet stability—by assessing meteoric beryllium-10 profiles in mid-Miocene and late Quaternary soils at three sites situated 1,200–1,800 metres above sea level in the McMurdo Dry Valleys. Interpreting these profiles as indicators of water infiltration, we find that meteoric beryllium-10 entered mid-Miocene soils as late as the late Miocene. Reconstructions based on palaeo-active-layer thickness and known thresholds of meteoric beryllium-10 mobility suggest late Miocene summer temperatures of 7–10 °C with annual precipitation >10 mm. Therefore, the high elevations have probably been under a hyper-arid polar climate since the late Miocene (~6 Ma) and not the middle Miocene (13.8–12.5 Ma) as indicated by some previous reconstructions. Together, our findings indicate that high elevations of the McMurdo Dry Valleys probably experienced warm and wet climatic intervals from ~14.0 to 6.0 Ma, which reconciles observations of coastal warmth and reduced ice in the Ross Embayment. This finding also suggests that the McMurdo Dry Valleys may be more susceptible to climate change than anticipated.

Antarctica has been a cold continent with permanent ice sheets since ~33.9 million years ago (Ma) (ref. 1). It has been suggested that following the Miocene Climatic Optimum (~17.0–14.8 Ma), a period when ice sheets decreased in volume and a tundra environment occupied some of the ice-free regions[2,3], the climate changed to cold and hyper-arid conditions during the middle Miocene climate transition (MMCT) at 14.8–13.8 Ma (refs. 2,4). This transition to a cold and dry climate also represents the maximum age obtained from surface-exposure

[1]Antarctic Research Centre, Victoria University of Wellington, Wellington, New Zealand. [2]Department of Arctic Geology, The University Centre in Svalbard, Svalbard and Jan Mayen, Norway. [3]School of Geography, Environment and Earth Sciences, Victoria University of Wellington, Wellington, New Zealand. [4]Department of Geography, Environment and Geomatics, University of Ottawa, Ottawa, Ontario, Canada. [5]Department of Physics, Laboratory of Ion Beam Physics, ETH Zürich, Zurich, Switzerland. [6]GNS Science, Lower Hutt, New Zealand. ✉e-mail: marjolainv@unis.no

https://doi.org/10.1038/s41561-023-01193-4

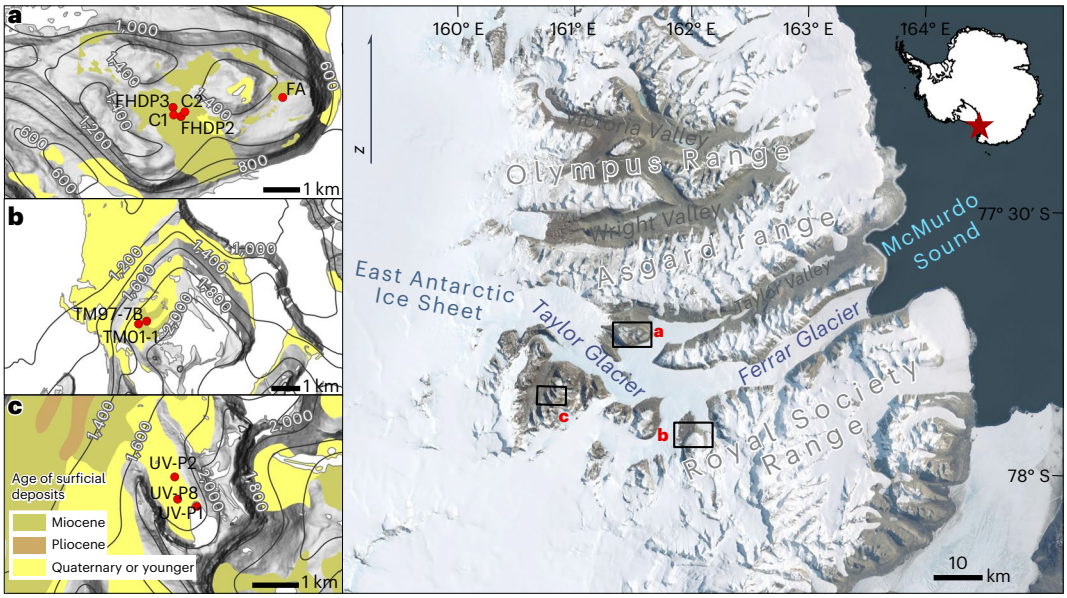

Fig. 1 | Location of the study sites in the MDVs. a, Friis Hills. **b**, Table Mountain. **c**, University Valley in the MDV of Antarctica. FHDP, Friis Hills Drilling Project; TM, Table Mountain; UV, University Valley. Digital elevation model from ref. 49. Antarctic outline and basemap from ref. 50. Geologic basemap from refs. 21,51.

dating at high elevations (>2,000 m above sea level (a.s.l.)) and was associated with limited weathering caused by the absence of surficial liquid water[5]. While the coastal zone in the Ross Embayment has experienced warm periods that coincide with sea-ice melt and retreat of the West Antarctic Ice Sheet during past interglacials[6], the high elevations of the McMurdo Dry Valleys (MDV), known as the stable uplands[7], are thought to have remained under a cold and hyper-arid climate since ~12.5–13.8 Ma (refs. 8–11). Assuming a persistent hyper-arid climate, some studies have suggested that the uppermost tens of metres of permafrost soils in the MDV should be largely free of ground ice due to its sublimation under hyper-arid climate[12]. However, other studies documented the widespread presence of ice-cemented permafrost soils that were inferred to have formed through infiltration and freezing of evaporated snowmelt, a finding that challenges the persistent aridity since the mid-Miocene[13–15].

Meteoric beryllium-10 ($^{10}Be_{met}$) is a tracer of water infiltration, and its migration in soils can be used to assess the onset of persistent aridity in the MDV and East Antarctica[11,16,17]. Meteoric ^{10}Be is formed in the upper atmosphere by cosmic ray-induced spallation of oxygen, producing ^{10}BeO and $^{10}Be(OH)_2$, which adhere to atmospheric aerosols and are transferred to Earth's surface by wet (rain or snow) or dry (dust) deposition[18]. Through continued deposition, $^{10}Be_{met}$ accumulates at the surface and, at most natural pH levels (pH > 4), adsorbs onto fine soil particles that are translocated below the surface by infiltration and clay illuviation[19]. This, along with the predictability of atmospheric flux, makes $^{10}Be_{met}$ a suitable environmental tracer of water movement and its residence time through soil profiles over million-year timescales[11,17]. Initial $^{10}Be_{met}$ profiles at Table Mountain, in the MDV, showed substantial $^{10}Be_{met}$ concentrations ([$^{10}Be_{met}$]) down to at least 4.5 m, which suggests infiltration of liquid water in the soils well after 12.5 Ma (ref. 17). However, a single measurement of $^{10}Be_{met}$ below the blank range at 60 cm of depth in mid-Miocene-age sediments in the nearby Friis Hills suggests persistent polar aridity since 12.5–13.8 Ma (ref. 11).

New data presented in this study allow us to reconcile the apparent conflict over the onset of polar aridity in the high-elevation regions of the MDV. In this article, we report 64 new $^{10}Be_{met}$ measurements from 10 boreholes obtained in mid-Miocene and late Quaternary-age icy permafrost soils at 3 sites in the upper MDV (Fig. 1). By using [$^{10}Be_{met}$] from boreholes at the two mid-Miocene sites, we constrain the timing and magnitude of water infiltration in these soils since the mid-Miocene and show that near-surface soils in the high elevations of the MDV have not remained frozen over the past 15 Myr.

Meteoric beryllium-10 in the MDV permafrost

The stable upland zone of the MDV is a cold and hyper-arid desert environment where maximum air temperatures remain below 0 °C, and precipitation is limited to ~3.0–14.0 mm snow water equivalent (s.w.e.) that quickly sublimates or is removed by katabatic winds[7,20]. Cores of frozen sediments were collected from three sites in this zone: Friis Hills, Table Mountain and University Valley (Fig. 1 and Extended Data Fig. 1). The Friis Hills (77° 45′ S, 161° 30′ E; 1,200–1,500 m a.s.l.) are a 12-km-wide inselberg at the head of Taylor Valley[21]. Surficial deposits at Friis Hills consist of an ~80-m-thick sequence of glacial drifts interbedded with lacustrine sediments, originating from the advance and retreat of a local alpine glacial system connected to the East Antarctic Ice Sheet[21]. The $^{40}Ar/^{39}Ar$ dating of tephra layers and palaeomagnetic reversal stratigraphy indicates the sequence spans the interval from ~15.0 to 14.0 Ma (ref. 22). The sediment therefore captures the transition from the end of the Miocene Climatic Optimum (~17.0–14.8 Ma) and the progressive cooling of the MMCT (14.8–13.8 Ma; Fig. 2)[2]. Table Mountain (77° 57′ S, 161° 57′ E; 1,800–1,945 m a.s.l) is located on the southern side of the Ferrar Glacier, bounded southwest by Tedrown Glacier and east by Emmanuel Glacier[23] (Fig. 1). Surficial deposits consist of Sirius Group sediments overlying Beacon Supergroup sediments. Although the age of the Sirius Group has been debated, stratigraphic relationships[8], $^{40}Ar/^{39}Ar$ dating of tephra layers[24] and cosmogenic exposure ages[25] indicate that the deposit at Table Mountain probably predates 15.0 Ma. University Valley (77° 52′ S, 160° 45′ E; 1,600–1,800 m a.s.l.) is a hanging glacial valley situated ~450 m above the floor of Beacon Valley with late Quaternary-age surficial sediments that originate from the weathering of the Beacon Supergroup sandstone[14] (Fig. 1). Surface sediments in University Valley comprising undifferentiated till and alpine drift are Quaternary in age on the basis of optically stimulated luminescence dating[26]. At all three sites, 20–70 cm of dry permafrost overlies ice-cemented permafrost that often contains ground ice above pore saturation[13–15]. Due to cold summers, an active layer <5 cm develops at these sites[27].

https://doi.org/10.1038/s41561-023-01193-4

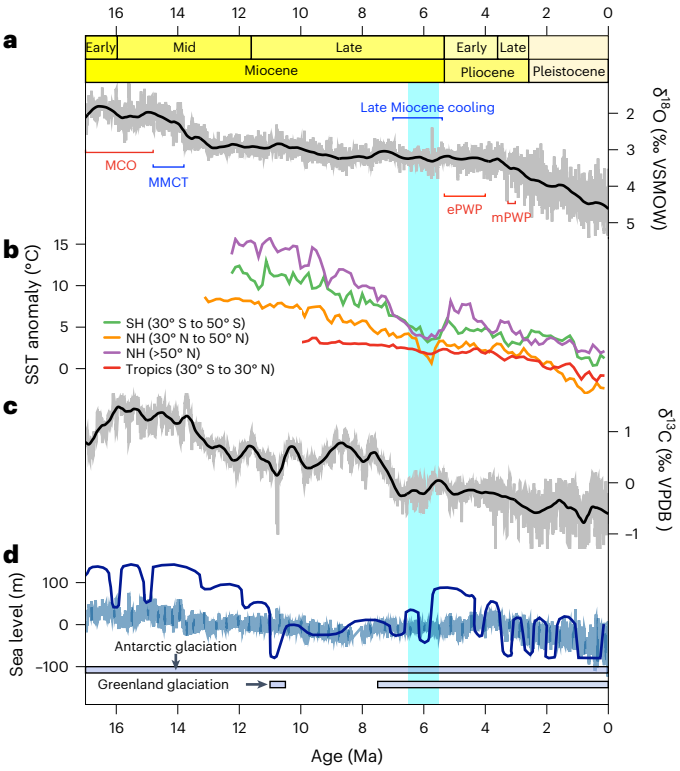

Fig. 2 | Compiled global and regional palaeoclimatic indicators of the past 17 Myr. a, Benthic foraminifera $\delta^{18}O$ (from carbonate-rich deep-sea sediments drilled during Ocean Drilling Program and Integrated Ocean Drilling Program expeditions) with locally weighted smoothing in black[52]. **b**, Regional sea surface temperature (SST) anomalies[44]. **c**, Benthic foraminifera $\delta^{13}C$ (from carbonate-rich deep-sea sediments drilled during Ocean Drilling Program and Integrated Ocean Drilling Program expeditions) with locally weighted smoothing in black[52]. **d**, Global mean sea-level estimates in dark blue (eustatic Haq sea-level curve)[53] and light blue[4] (on the basis of benthic foraminifera $\delta^{18}O$). Major warming events (red brackets) and major cooling events (blue brackets) are labelled, and Greenland[54] and Antarctic[1] glaciations are labelled. Onset of permanent polar aridity in East Antarctica according to this study is indicated with teal panel. MCO, Miocene Climatic Optimum; ePWP, early Pliocene warm period; mPWP, mid-Pliocene warm period; NH, Northern Hemisphere; SH, Southern Hemisphere; VPDB, Vienna PeeDee Belemnite; VSMOW, Vienna standard mean ocean water.

Average surface [$^{10}Be_{met}$] is 1.06×10^8 atoms g^{-1} at Friis Hills (sites 2C, C2 and FA; Extended Data Tables 1 and 3), 4.75×10^8 atoms g^{-1} at Table Mountain (Extended Data Table 3) and 1.19×10^9 atoms g^{-1} at University Valley (Extended Data Table 2). The order of magnitude increase at University Valley is probably due to the morphology of the valley, which makes it a better catchment for $^{10}Be_{met}$-rich dust and aerosols than other sites in the MDV that are exposed to katabatic winds (such as Friis Hills and Table Mountain)[16]. At all sites, [$^{10}Be_{met}$] decreases by one to two orders of magnitude immediately below the surface, but concentrations remain above analytical blank (Fig. 3a). The [$^{10}Be_{met}$] profiles in the Miocene sites, Friis Hills and Table Mountain, displayed similar trends with depth. The $^{10}Be_{met}$ profiles were separated into three groups (near surface, intermediate and deep) with the boundary between near-surface and intermediate groups at 227 cm at Friis Hills and 349 cm at Table Mountain (Figs. 3b and 4a). The [$^{10}Be_{met}$] depth profile within the near-surface group can be defined by equation $y = 5.03 \times 10^6 \times e^{-0.0108x}$ ($r^2 = 0.92$) at Friis Hills and $y = 2.50 \times 10^7 \times e^{-0.0116x}$ ($r^2 = 0.93$) at Table Mountain (Fig. 4). The [$^{10}Be_{met}$] within the intermediate group reached a steady value of $4.26 \times 10^5 \pm 9.95 \times 10^4$ atoms g^{-1} at Friis Hills and $4.45 \times 10^5 \pm 2.15 \times 10^5$ atoms g^{-1} at Table Mountain (Fig. 4a). The [$^{10}Be_{met}$] in the deep group (below 35 m at Friis Hills) were statistically lower than in the intermediate group samples ($P < 0.05$), varying between 1.33×10^5 and 4.31×10^5 atoms g^{-1} (average 2.10×10^5 atoms g^{-1}; Fig. 3b).

Onset of polar aridity in the MDV

The abrupt decrease in [$^{10}Be_{met}$] of one to two orders of magnitude directly below the surface at all sites suggests little to no disturbance of the soils at least throughout the late Quaternary. The high [$^{10}Be_{met}$] directly below the surface at Friis Hills and Table Mountain, which are on the order of 10^7 atoms g^{-1}, suggest transport of $^{10}Be_{met}$ in the soils after the MMCT. For example, on the basis of the decay rate of ^{10}Be, the immediate subsurface concentration of 10^7 atoms g^{-1} would have been on the order of 10^{10} atoms g^{-1} 14.5 Ma. This [$^{10}Be_{met}$] is higher than measured anywhere on Earth (and would require a production rate higher than the maximum current global production rate), which indicates that the subsurface $^{10}Be_{met}$ has been there less than 14.5 Ma. We therefore solve for the closure age (the time when $^{10}Be_{met}$ stopped infiltrating the ground and was sealed off in the sediment profile; Fig. 4b) using conservative assumptions and conservative erosion rates (Methods). The $^{10}Be_{met}$ decay curves at Friis Hills and Table Mountain suggest two active periods of water infiltration: the sediments above 227 cm at Friis Hills and above 349 cm at Table Mountain both closed off at ~6.0 ± 0.5 Ma; the intermediate sections closed off at the latest ~12.0 Ma at Friis Hills and at the latest ~16.0 Ma at Table Mountain; and the samples below 40 m at Friis Hills were sealed off from surface infiltration at the latest ~14.0 Ma. Since the calculation for the closure age requires several assumptions (Methods), the calculated closure ages probably represent the lower age limit. Nevertheless, the conclusion remains the same: water infiltrated these high-elevation sites of the MDV after the MMCT.

In sediments, $^{10}Be_{met}$ is transported by (1) mechanical transport of $^{10}Be_{met}$ absorbed to clays, which translocate by percolating water, or (2) solutional transport of $^{10}Be_{met}$ if soil pH is <3 (ref. 28). Solutional transport at our sites can be ruled out as soil pH generally ranges between 7.5 and 9.5 in the MDV[29], and while lower pH values of 5–6 are recorded in highly nitric soils[29], they are still too alkaline to support solutional transport. As such, $^{10}Be_{met}$ is mechanically transported in these soils. Unfrozen water in permafrost sediments can migrate under thermal-stress gradients and Van der Waals force[30]. However, this unfrozen water cannot translocate clays and hence mobilize $^{10}Be_{met}$ (ref. 19). Therefore, the presence of $^{10}Be_{met}$ at depth at the two Miocene-age study sites requires translocation under conditions where an active layer developed above the permafrost. The transport of $^{10}Be_{met}$ in an active layer requires a climate that is warmer and wetter than today. At Friis Hills, the similar $^{40}Ar/^{39}Ar$ ages of tephras in the sediments (~5–27 m; 14.0–15.0 Ma) and the $^{10}Be_{met}$ closure ages in the deep groups (~30–40 m; <14.0 Ma) imply that the infiltration of water could have happened more or less simultaneously with the deposition of the sediments and near-synchronous aggradation of permafrost[15]. The same inference can be made from the Table Mountain site, where the maximum closure age of ~16.0 Ma coincides with the mid-Miocene age of the sediment (~15.0 Ma). However, the near-surface regolith at Friis Hills and Table Mountain (~2–3.5 m) likely closed off during the late Miocene, which challenges the assumption that the high elevations of the MDV remained frozen under a cold and hyper-arid climate since the MMCT. A late Miocene closure age suggests that the mid- to late Miocene was either (1) continuously favourable to water infiltration and translocation of clays in an active layer or (2) mostly under cold and dry conditions but punctuated with warmer wetter intervals. Surface-exposure dating from sites at a similar elevation to Table Mountain and Friis Hills (1,000–1,500 m a.s.l.) across Antarctica seems to support the second scenario with enhanced erosion at specific time intervals (for example, an ~250 kyr period favourable to erosion at ~5.0 Ma) (ref. 5). Nevertheless, in either scenario, the conditions that allow translocation of clays in soils stopped during the late Miocene, after which the climate remained under persistent polar aridity.

https://doi.org/10.1038/s41561-023-01193-4

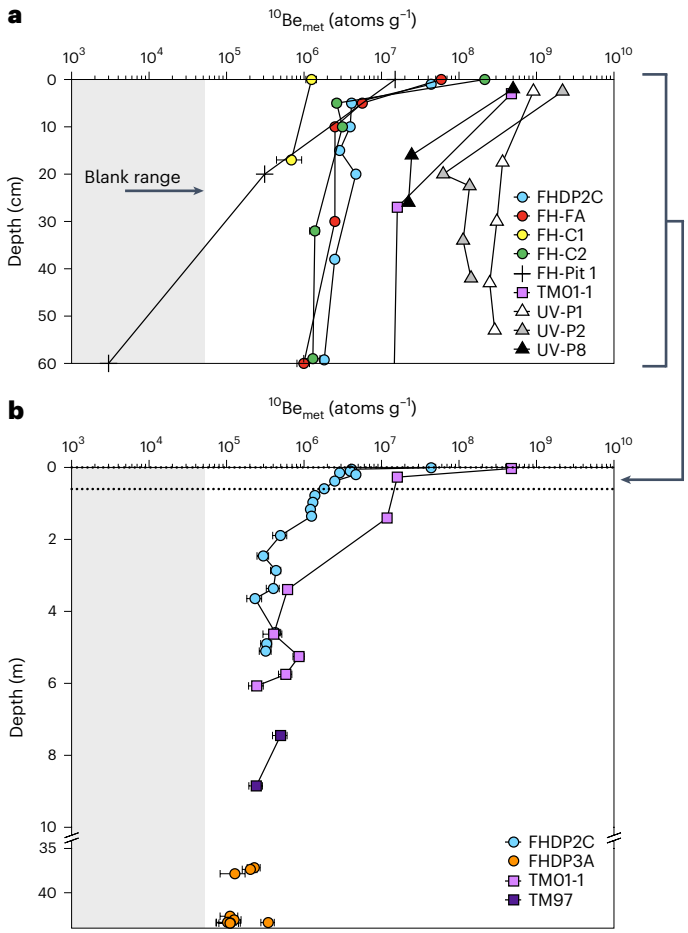

Fig. 3 | $^{10}Be_{met}$ concentration profiles in high-elevation sites of the MDV. a, The $^{10}Be_{met}$ concentrations measured at shallow depths at Friis Hills, Table Mountain and University Valley compared with Friis Hills Pit 1 (ref. 11). **b**, The $^{10}Be_{met}$ concentrations measured in both shallow and deep Miocene sites. FHDP2C and FHDP3A from Friis Hills and TM01 and TM97 from Table Mountain. The dotted line represents the depth of **a**; the grey panel shows the blank range. Error bars are expressed for each sample on the basis of analytical error (Extended Data Tables 1–3).

Climate and soil conditions that allow the translocation of $^{10}Be_{met}$ in soils are poorly defined, especially for cold hyper-arid environments, since they depend heavily on micro-scale mechanical processes. Conceptual models on colloid mobility in unsaturated sediments suggest that a critical water content is needed for initiation of mobilization[31]. A study from the warm hyper-arid Atacama Desert in Chile, where mean annual precipitation is <2 mm, similar to the upper MDV, found that $^{10}Be_{met}$ was not translocated in soils under modern conditions, but translocation was possible during wetter El Niño events, when precipitation was 4.6 times greater[32]. By analogy, the lack of evidence for $^{10}Be_{met}$ translocation in the near-surface soils in the stable upland sites suggests that precipitation has been <10 mm s.w.e. since the late Miocene, a value similar to contemporary precipitation. However, water may infiltrate the soils without $^{10}Be_{met}$ translocation. For example, in places where the ground surface warms above 0 °C for a few hours, such as in University Valley, snowmelt was observed to infiltrate the dry permafrost and reach the shallow ice table[14], although the $^{10}Be_{met}$ profile shows minimal subsurface mixing. Further evidence of snowmelt infiltrating and freezing at some depth in soils comes from the $\delta^{18}O$ and D-excess profiles of the near-surface ground ice at University Valley, Friis Hills and Table Mountain[13–15]. The $\delta^{18}O$ profiles of ground ice at the three sites are very similar, which suggests that the near-surface icy permafrost is dynamic and responds synchronously to the late Quaternary climatic changes[13–15]. Therefore, infiltrating snowmelt occurs during contemporary times and contributes to developing the ground ice; however, the amount of precipitation, or snowmelt, has been insufficient (probably <10 mm s.w.e.) to translocate $^{10}Be_{met}$ in the dry permafrost soils since the late Miocene.

Palaeoclimate reconstruction during the late Miocene

The presence of $^{10}Be_{met}$ and the profile inflection at 227 cm at Friis Hills and 349 cm at Table Mountain suggests that the sites had an active layer with enough precipitation for the translocation of clays in the soils until the late Miocene. Considering that the translocation of clays does not occur in permafrost, we assume that the profile inflection depths represent the thickness of the active layer at the calculated closure age of ~6.0 ± 0.5 Ma. The thicker active layer at Table Mountain could be attributed to the coarser material and lower organic-matter content, which would in turn have greater thermal conductivity (up to 4.1 ± 0.4 W m^{-1} °C^{-1} in quartz-rich samples[33]). After correcting for the vertical erosion since 6.0 Ma, calculated from erosion rates at each site (~57 cm at Friis Hills and ~7 cm at Table Mountain), and removing the volume added by the growth of excess ice in the permafrost (~10 cm at both sites)[34], the maximum active-layer thickness was 274 cm at Friis Hills and 345 cm at Table Mountain at ~6.0 ± 0.5 Ma. Currently, Antarctic active-layer thicknesses range from ~1 m along the coastal regions to ~5 cm in the upper elevations[35], and a strong relation exists between active-layer thickness and the mean annual air temperature (MAAT; $y = 13{,}077 \times e^{0.3052x}$; $r^2 = 0.80$), and mean summer air temperature (MSAT; $y = 98.925 \times e^{0.1952x}$; $r^2 = 0.72$).

The PERICLIMv1.0 model[36], which includes thawed-ground thermal conductivity, soil moisture and ground-surface thawing *n*-factor as parameters, was used to estimate air temperatures on the basis of the active-layer thickness through inverse solution of the Stefan equation (Extended Data Fig. 4 and Extended Data Table 4)[36]. The PERICLIM model was first able to reproduce the modern active-layer thickness in the MDV solely by varying the annual air temperature amplitude, with values of ground thermal parameters typical of nearly dry soils and kept constant between the sites (Extended Data Fig. 4). To estimate air temperatures during the late Miocene, the ground thermal parameters were adjusted for typical near-saturated active layer with fine-sand soils, and considering that there is no evidence of vegetation at these sites since the mid-Miocene[37], the value of the thawing *n*-factor was set to represent a surface with no organic layer or vegetation cover. On the basis of the palaeo-active-layer thickness estimated from [$^{10}Be_{met}$] (274 cm at Friis Hills and 345 cm at Table Mountain), the PERICLIM model predicts a MAAT ranging between −11 and −8 °C and an MSAT in the 7–10 °C range, which are much warmer than the modern MAAT and MSAT of −22 °C and −13 °C, respectively[38]. These reconstructed air temperatures and active-layer thickness at ~6.0 ± 0.5 Ma for the stable upland zone of the MDV are comparable to modern environments in highland mid-Arctic, such as west Greenland[39], although palaeo-active layers at Friis Hills and Table Mountain are probably thicker due to absence of organic matter and vegetation cover.

Considering the lapse rate, the palaeo-air temperature reconstruction in the high elevations at ~6.0 ± 0.5 Ma is in line with other regional proxies from the coastal regions and provides evidence that the late Miocene warm and wet interval(s) extended to the high elevations of the MDV, with the onset of permanent polar aridity starting only during the late Miocene. For example, MSAT during the Neogene in lower Taylor Valley (80 m a.s.l.; Fig. 1) were ~5 °C with a transition to cooler conditions occurring between 4.1 and 2.6 Ma (ref. 40). A similar MSAT was reconstructed on the basis of lipid biomarkers at

https://doi.org/10.1038/s41561-023-01193-4

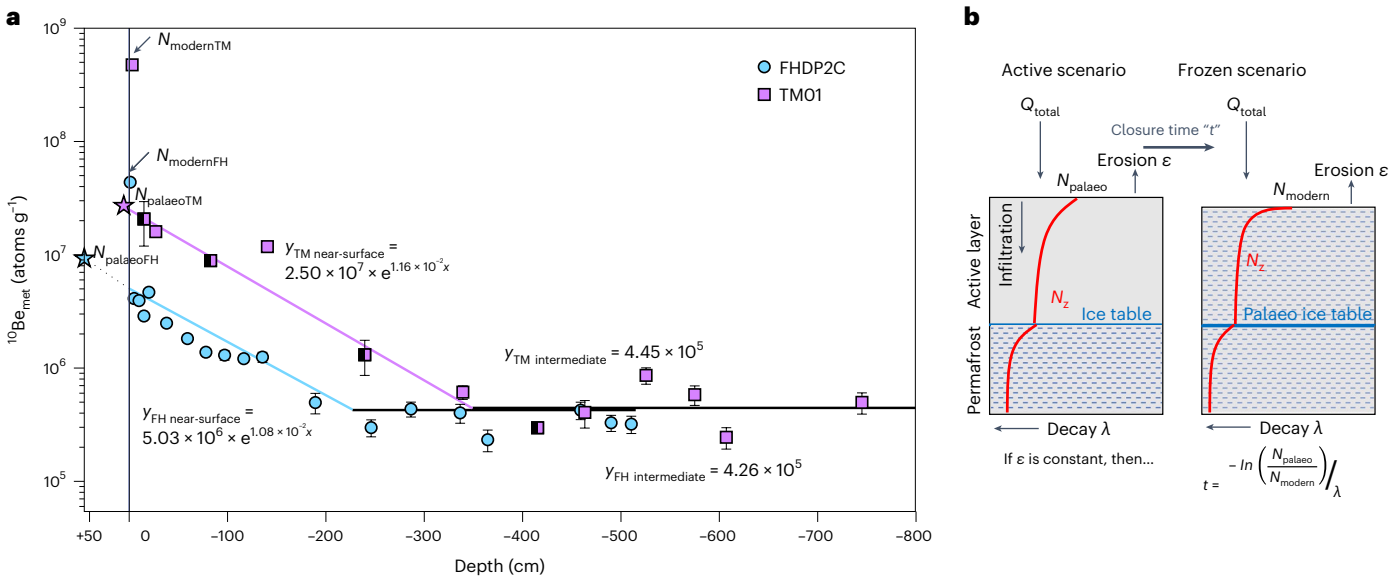

Fig. 4 | Modelling palaeosurface concentrations of $^{10}Be_{met}$ to solve for closure age. a, Exponential regression equations for measured $^{10}Be_{met}$ concentrations of FHDP2C and TM01-1 and TM97 in subsurface profiles for upper (fit line matching data points) and intermediate sample groups (black fit lines). Segmentation at 227 cm depth in Friis Hills samples and 349 cm depth in Table Mountain samples. Note: half-black markers in the TM01 dataset are corrected from ref. 17. Error bars are expressed for each sample on the basis of analytical error (Extended Data Tables 1–3). See details in Methods and Extended Data Figs. 2 and 3. *y* represents the concentration of $^{10}Be_{met}$ (in atoms per gram) and *x* represents depth (in centimetre). **b**, Schematic representation of a $^{10}Be_{met}$ ground profile. The active scenario, where $^{10}Be_{met}$ infiltration occurs is compared with the frozen scenario where $^{10}Be_{met}$ accumulates at the surface. Closure age represents the time since the system has been sealed off from infiltration. N_{modern} is the modern surface concentration of $^{10}Be_{met}$ (in atoms per gram), N_{palaeo} is the palaeo-surface concentration of $^{10}Be_{met}$ (in atoms per gram), N_z is the concentration of $^{10}Be_{met}$ (in atoms per gram) with depth and Q_{total} is the flux of $^{10}Be_{met}$ (in atoms per square centimetre per year).

Oliver Bluffs (850 km south of the MDV), which also allowed the existence of a low-diversity tundra plant community[41]. At the continental-scale, long-term temperature records throughout the Neogene suggest summer temperatures ranged between 4 and 12 °C (ref. 3). Evidence supporting a warm and wet late Miocene period and melting of glacial ice is found in various coastal regions, such as the Ross Embayment[6], Prydz Bay[42] and the Totten Glacier region[43].

Continental-scale response to polar aridity

The timing of permanent polar aridity across the MDV is critical to our understanding of the overall response of cryosphere systems in Antarctica, including the East Antarctic Ice Sheet. Although proxy data show surface temperatures remained substantially warmer through the late Miocene than today[44–46], the hypothesis that the upper elevations remained under a hyper-arid polar climate since the MMCT has persisted. This study analysed $^{10}Be_{met}$ from more than 64 samples collected at three locations in the upper MDV and 10 different boreholes, using 2 chemical protocols and 2 different AMS laboratories (Methods). The results suggest that $^{10}Be_{met}$ infiltrated the ground for a period between the mid-Miocene and the late Miocene, which supports the presence of liquid water post-MMCT with the onset of polar aridity starting well after previous reconstructions. This finding provides strong evidence that the climatic conditions have not remained stable since the MMCT and corroborates regional evidence that suggests the Antarctic Ice Sheet became larger, drier and less dynamic during the late Miocene[47]. The onset of permanent polar aridity in the high elevation of the MDV (at least 1,500 m a.s.l.) during the late Miocene coincides with a 2 to 3 °C decrease in ocean surface temperatures in the Southern Ocean between 7.0 and 5.4 Ma (ref. 44) (Fig. 1). This late Miocene cooling is also synchronous with late Miocene aridity and terrestrial ecosystem changes with increasing meridional temperature gradients[48]. Most important, this finding implies that the MDV are not a landscape frozen in time, and they may be more susceptible to climate change than anticipated.

Online content

Any methods, additional references, Nature Portfolio reporting summaries, source data, extended data, supplementary information, acknowledgements, peer review information; details of author contributions and competing interests; and statements of data and code availability are available at https://doi.org/10.1038/s41561-023-01193-4.

References

1. Coxall, H. K., Wilson, P. A., Pälike, H., Lear, C. H. & Backman, J. Rapid stepwise onset of Antarctic glaciation and deeper calcite compensation in the Pacific Ocean. *Nature* **433**, 53–57 (2005).
2. Zachos, J. C., Dickens, G. R. & Zeebe, R. E. An early Cenozoic perspective on greenhouse warming and carbon-cycle dynamics. *Nature* **451**, 279–283 (2008).
3. Warny, S. et al. Palynomorphs from a sediment core reveal a sudden remarkably warm Antarctica during the middle Miocene. *Geology* **37**, 955–958 (2009).
4. Miller, K. G. et al. Cenozoic sea-level and cryospheric evolution from deep-sea geochemical and continental margin records. *Sci. Adv.* **6**, aaz1346 (2020).
5. Spector, P. & Balco, G. Exposure-age data from across Antarctica reveal mid-Miocene establishment of polar desert climate. *Geology* **49**, 91–95 (2021).
6. McKay, R. et al. The stratigraphic signature of the late Cenozoic Antarctic Ice Sheets in the Ross Embayment. *Geol. Soc. Am. Bull.* **121**, 1537–1561 (2009).
7. Marchant, D. & Head, J. W. III Antarctic Dry Valleys: microclimate zonation, variable geomorphic processes, and implications for assessing climate change on Mars. *Icarus* **192**, 187–222 (2007).
8. Denton, G. H., Sugden, D. E., Marchant, D., Hall, B. L. & Wilch, T. I. East Antarctic Ice Sheet sensitivity to Pliocene climatic change from a Dry Valleys perspective. *Geogr. Ann. A* **75**, 155–204 (1993).

9. Sugden, D. E. et al. Preservation of Miocene glacier ice in East Antarctica. *Nature* **376**, 412–414 (1995).
10. Summerfield, M. et al. Long-term rates of denudation in the Dry Valleys, Transantarctic Mountains, southern Victoria Land, Antarctica based on in-situ-produced cosmogenic ^{21}Ne. *Geomorphology* **27**, 113–129 (1999).
11. Valletta, R. D., Willenbring, J. K., Lewis, A. R., Ashworth, A. C. & Caffee, M. Extreme decay of meteoric Beryllium-10 as a proxy for persistent aridity. *Sci. Rep.* **5**, 17813 (2015).
12. Hindmarsh, R., Van der Wateren, F. & Verbers, A. L. Sublimation of ice through sediment in Beacon Valley, Antarctica. *Geogr. Ann. A* **80**, 209–219 (1998).
13. Dickinson, W. W. & Rosen, M. R. Antarctic permafrost: an analogue for water and diagenetic minerals on Mars. *Geology* **31**, 199–202 (2003).
14. Lacelle, D. et al. Excess ground ice of condensation–diffusion origin in University Valley, Dry Valleys of Antarctica: evidence from isotope geochemistry and numerical modeling. *Geochim. Cosmochim. Acta* **120**, 280–297 (2013).
15. Verret, M. et al. Cryostratigraphy of mid-Miocene permafrost at Friis Hills, McMurdo Dry Valleys of Antarctica. *Antarct. Sci.* **33**, 174–188 (2020).
16. Schiller, M., Dickinson, W., Ditchburn, R., Graham, I. & Zondervan, A. Atmospheric ^{10}Be in an Antarctic soil: implications for climate change. *J. Geophys. Res. Earth Surf.* **114**, F01033 (2009).
17. Dickinson, W. W., Schiller, M., Ditchburn, B. G., Graham, I. J. & Zondervan, A. Meteoric Be-10 from Sirius Group suggests high elevation McMurdo Dry Valleys permanently frozen since 6 Ma. *Earth Planet. Sci. Lett.* **355**, 13–19 (2012).
18. McHargue, L. & Damon, P. The global beryllium-10 cycle. *Rev. Geophys.* **29**, 141–158 (1991).
19. Willenbring, J. K. & von Blanckenburg, F. Meteoric cosmogenic beryllium-10 adsorbed to river sediment and soil: applications for Earth-surface dynamics. *Earth Sci. Rev.* **98**, 105–122 (2010).
20. Fountain, A., Nylen, T. H., Monaghan, A., Basagic, H. J. & Bromwich, D. Snow in the McMurdo Dry Valleys, Antarctica. *Int. J. Climatol.* **30**, 633–642 (2010).
21. Lewis, A. R. & Ashworth, A. C. An early to middle Miocene record of ice-sheet and landscape evolution from the Friis Hills, Antarctica. *Geol. Soc. Am. Bull.* **128**, 719–738 (2015).
22. Chorley, H. et al. East Antarctic Ice Sheet variability during the middle Miocene Climate Transition captured in drill cores from the Friis Hills, Transantarctic Mountains. *Geol. Soc. Am. Bull.* **135**, 1503–1529 (2022).
23. Goff, J. R., Jennings, I. W. & Dickinson, W. W. Depositional environment of Sirius Group sediments, Table Mountain, Dry Valleys area, Antarctica. *Geogr. Ann. A* **84**, 11–24 (2002).
24. Marchant, D., Denton, G., Swisher, C. C. III & Potter, N. Jr Late Cenozoic Antarctic paleoclimate reconstructed from volcanic ashes in the Dry Valleys region of southern Victoria Land. *Geol. Soc. Am. Bull.* **108**, 181–194 (1996).
25. Ivy-Ochs, S., Schlüchter, C., Kubik, P. W., Dittrich-Hannen, B. & Beer, J. Minimum ^{10}Be exposure ages of early Pliocene for the Table Mountain plateau and the Sirius Group at Mount Fleming, Dry Valleys, Antarctica. *Geology* **23**, 1007–1010 (1995).
26. Trinh-Le, C. A. *Dry Sedimentation Processes in the High-Elevation McMurdo Dry Valleys, Antarctica: A Case Study in University Valley*. MSc thesis, Victoria Univ. Wellington (2017).
27. Lacelle, D. et al. Solar radiation and air and ground temperature relations in the cold and hyper-arid Quartermain Mountains, McMurdo Dry Valleys of Antarctica. *Permafr. Periglac. Process.* **27**, 163–176 (2016).
28. Takahashi, Y., Minai, Y., Ambe, S., Makide, Y. & Ambe, F. Comparison of adsorption behavior of multiple inorganic ions on kaolinite and silica in the presence of humic acid using the multitracer technique. *Geochim. Cosmochim. Acta* **63**, 815–836 (1999).
29. Campbell, I. & Claridge, G. *Antarctica: Soils, Weathering Processes and Environment* (Elsevier, 1987).
30. Fisher, D. A., Lacelle, D., Pollard, W. & Faucher, B. A model for stable isotopes of residual liquid water and ground ice in permafrost soils using arbitrary water chemistries and soil-specific empirical residual water functions. *Permafr. Periglac. Process.* **32**, 248–260 (2020).
31. Shang, J., Flury, M., Chen, G. & Zhuang, J. Impact of flow rate, water content, and capillary forces on in situ colloid mobilization during infiltration in unsaturated sediments. *Water Resour. Res.* **44**, W06411 (2008).
32. Wang, F. et al. Beryllium-10 concentrations in the hyper-arid soils in the Atacama Desert, Chile: implications for arid soil formation rates and El Niño driven changes in Pliocene precipitation. *Geochim. Cosmochim. Acta* **160**, 227–242 (2015).
33. Pringle, D., Dickinson, W., Trodahl, H. & Pyne, A. Depth and seasonal variations in the thermal properties of Antarctic Dry Valley permafrost from temperature time series analysis. *J. Geophys. Res. Solid Earth* **108**, 1–12 (2003).
34. Burn, C. R. Cryostratigraphy, paleogeography, and climate change during the early Holocene warm interval, western Arctic coast, Canada. *Can. J. Earth Sci.* **34**, 912–925 (1997).
35. Adlam, L. S., Balks, M. R., Seybold, C. A. & Campbell, D. I. Temporal and spatial variation in active layer depth in the McMurdo Sound Region, Antarctica. *Antarct. Sci.* **22**, 45–52 (2010).
36. Uxa, T., Křížek, M. & Hrbáček, F. PERICLIMv1.0: a model deriving palaeo-air temperatures from thaw depth in past permafrost regions. *Geosci. Model Dev.* **14**, 1865–1884 (2021).
37. Lewis, A. et al. Mid-Miocene cooling and the extinction of tundra in continental Antarctica. *Proc. Natl Acad. Sci. USA* **105**, 10676–10680 (2008).
38. Fountain, A. & Doran, P. McMurdo Dry Valleys Friis Hills Meteorological Station daily averages, version 5. *Environmental Data Initiative* https://doi.org/10.6073/pasta/9dda244e95ce8dfcdbd9b94d2289ef1d (2016).
39. Van Tatenhove, F. G. & Olesen, O. B. Ground temperature and related permafrost characteristics in West Greenland. *Permafr. Periglac. Process.* **5**, 199–215 (1994).
40. Ohneiser, C. et al. Warm fjords and vegetated landscapes in early Pliocene East Antarctica. *Earth Planet. Sci. Lett.* **534**, 116045 (2020).
41. Rees-Owen, R. L. et al. The last forests on Antarctica: reconstructing flora and temperature from the Neogene Sirius Group, Transantarctic Mountains. *Org. Geochem.* **118**, 4–14 (2018).
42. Hambrey, M. J. & McKelvey, B. Major Neogene fluctuations of the East Antarctic Ice Sheet: stratigraphic evidence from the Lambert Glacier region. *Geology* **28**, 887–890 (2000).
43. Gulick, S. P. et al. Initiation and long-term instability of the East Antarctic Ice Sheet. *Nature* **552**, 225–229 (2017).
44. Herbert, T. D. et al. Late Miocene global cooling and the rise of modern ecosystems. *Nat. Geosci.* **9**, 843–847 (2016).
45. Prebble, J. G. et al. Terrestrial climate evolution in the Southwest Pacific over the past 30 million years. *Earth Planet. Sci. Lett.* **459**, 136–144 (2017).
46. Super, J. R. et al. Miocene evolution of North Atlantic sea surface temperature. *Paleoceanogr. Paleoclimatol.* **35**, 1e2019PA003748 (2020).
47. Shakun, J. D. et al. Minimal East Antarctic Ice Sheet retreat onto land during the past eight million years. *Nature* **558**, 284–287 (2018).
48. Schuster, M. et al. The age of the Sahara desert. *Science* **311**, 821–821 (2006).
49. Howat, I. M., Porter, C., Smith, B. E., Noh, M.-J. & Morin, P. The reference elevation model of Antarctica. *Cryosphere* **13**, 665–674 (2019).
50. Antarctic Imagery. *Esri, Earthstar Geographics* http://goto.arcgisonline.com/maps/Antarctic_Imagery (2020).

51. Cox, S. et al. The GeoMAP (v.2022-08) continent-wide detailed geological dataset of Antarctica. *PANGAEA* https://doi.org/10.1594/PANGAEA.951482 (2022).
52. Westerhold, T. et al. An astronomically dated record of Earth's climate and its predictability over the last 66 million years. *Science* **369**, 1383–1387 (2020).
53. Miller, K. et al. The Phanerozoic record of global sea-level change. *Science* **310**, 1293–1298 (2005).
54. Bierman, P. R., Shakun, J. D., Corbett, L. B., Zimmerman, S. R. & Rood, D. H. A persistent and dynamic East Greenland Ice Sheet over the past 7.5 million years. *Nature* **540**, 256–260 (2016).

Methods

Field seasons and sample preparation

Table Mountain samples were collected from cores drilled during the 1996–1997 (TM97-7B) and 2000–2001 (TM01-1) field seasons led by researchers of the Victoria University of Wellington and with logistical support from Antarctica New Zealand (Extended Data Fig. 1a). University Valley cores (UV-P1, P2 and P8) were drilled in polygonal ground in January 2013 by researchers from the NASA (National Aeronautics and Space Administration) Ames Research Center and the University of Ottawa (Extended Data Fig. 1d). In December 2014, three preliminary cores were collected for a $^{10}Be_{met}$ survey at Friis Hills. Additional samples were selected from cores of the 2016 Friis Hills Drilling Project (FHDP2C and FHDP3A) led by researchers of the Victoria University of Wellington (Extended Data Fig. 1c). The samples selected were the following: 8 samples from TM01-1 (0–6 m depth), 2 samples from core TM97-7B (7–9 m depth), 13 samples from the University Valley cores (P1, P2 and P8; <50 cm depth), 12 samples from the Friis Hills preliminary cores (C1, C2 and FA; <60 cm), 19 samples from FHDP2C (0–5 m depth) and 10 samples from FHDP3A (37–44 m depth) for a total of 64 samples. All sediment samples were manually dry sieved to 45–90 µm and precisely weighted between 0.75 and 1.00 g into 50 ml centrifuge tubes before undergoing the sequential extraction procedure.

From $^{10}Be_{met}$ extraction to target packing

The method used in this paper follows the extraction method described in ref. 55 (adapted from refs. 56–58). Sequential extraction was performed on batches of 11 samples plus a chemical blank. Amorphous oxide-bound beryllium ($Be_{am\text{-}ox}$) was first extracted by adding 10 ml of 0.5 M HCl and gently shaking at room temperature for 24 h. The crystalline oxide-bound beryllium ($Be_{x\text{-}ox}$) was extracted second by adding 10 ml of 1 M hydroxylamine-hydrochloride solution (in 1 M HCl) and placing the samples in an ultrasonic bath at 80 °C for 4 h, shaking occasionally. Hydroxylamine-hydrochloride removal was done by a series of 10 ml concentrated HNO_3 and 10 ml 30% H_2O_2 washes. The solution with both $Be_{am\text{-}ox}$ and $Be_{x\text{-}ox}$ leachates was dried and then dissolved in 10 ml 3 M HNO_3. A 0.5 ml subsample was retrieved for aliquots of major and minor element analysis and for ^9Be measurement. A ^9Be carrier solution of ~0.9 g (305 ppm in 3 M HNO_3) was added to the solution, which was passed through Fe columns (2 ml Biorad 1-X8 100–200 mesh anion resin in 15 ml Eichrom columns) and Be columns (5 ml Biorad AG50-X8 200–400 mesh cation resin in 15 ml Eichrom columns).

To precipitate $Be(OH)_2$, 0.550 ml of concentrated (25%) NH_4OH was added to the samples taken up in 5 ml 1 M HNO_3 (to reach a pH of ~9). The samples were centrifuged and decanted, and the precipitates were redissolved in 5 ml 1 M HNO_3. This step was repeated a second time, and a final 3 ml Milli-Q H_2O wash was performed to remove ammonia from the $Be(OH)_2$ precipitates. The $Be(OH)_2$ precipitates were then dissolved in 0.3 ml of 5 M HNO_3, transferred to quartz crucibles and dried down at 120 °C. The samples were subsequently calcined for 1–2 min over open flame to form BeO. Niobium (~3 mg) was incorporated to form a homogeneous powder. The powder was then transferred into accelerator mass spectrometer (AMS) aluminium targets.

AMS measurement and sample calibration

Samples from preliminary cores FA, C1 and C2 and University Valley were measured on the 500 kV AMS (TANDY, ETH Zürich, 2017–2018) while FHDP2C, FHDP3A, TM01 and TM97 samples were measured on the 300 kV AMS (MILEA, ETH Zürich, 2019). The measured $^{10}Be/^9Be$ ratios were normalized using the 2007S and S2010N standards with nominal values of $^{10}Be/^9Be = 28.1 \times 10^{-12}$ and $^{10}Be/^9Be = 3.3 \times 10^{-12}$, respectively[59]. The 1σ errors of S2007N and S2010N are 2.7% and 2.2%, respectively. The concentration of $^{10}Be_{met}$ (atoms g^{-1}) per sample was determined with the following equation:

$$C_{^{10}Be_{met}} = \frac{\left(\frac{N_0 \times m_{^9Be_{carrier}}}{M(^9Be)}\right) \times \left(\frac{^{10}Be_{met}}{^9Be}\right)_{measured} - {}^{10}Be_{met}\ blank}{m_{sample}} \quad (1)$$

where $(^{10}Be_{met}/^9Be)_{measured}$ is the measured and standard normalized ratio of $^{10}Be_{met}$ to ^9Be measured directly from the sample, N_0 is Avogadro's number (6.022×10^{23} mol^{-1}), $m_{^9Be_{carrier}}$ is the mass of ^9Be in the added carrier solution (g), M(^9Be) is the molar mass of ^9Be (g mol^{-1}) and $^{10}Be_{met}$ blank is the number of ^9Be atoms added by the carrier solution multiplied by the $^{10}Be/^9Be$ ratio measured in chemical blank samples. The samples were corrected with the chemical blank associated with each batch (Extended Data Tables 1–3). To ensure that $^{10}Be_{met}$ measurements were independent of grain-size distribution[55], the stable isotope ^9Be was measured on the aliquot retrieved during the extraction process on an Agilent Microwave Plasma Atomic Emission Spectrometry (MP-AES) instrument model 4210 (University of Canterbury, School of Physical and Chemical Sciences). Concentrations in parts per million were measured with a standard error of ±15%. Concentrations of ^9Be measured independently on the MP-AES varied between 9.6×10^{16} and 3.0×10^{17} atoms g^{-1}. When normalized to ^9Be, $^{10}Be_{met}$ values were found to be highly correlated to non-normalized $^{10}Be_{met}$ values, implying that the reported $^{10}Be_{met}$ concentrations are not grain-size dependant (Extended Data Fig. 2).

Correction of Table Mountain samples

The study of $^{10}Be_{met}$ at Table Mountain by ref. 17 along with other early $^{10}Be_{met}$ investigations in the MDV[16,60,61] used a more aggressive leaching method to extract $^{10}Be_{met}$ from the sediment (6 M HCl for 1 h at 100 °C)[62,63]. This method was criticized because of the possibility of liberating in situ ^{10}Be via partial decomposition of clay minerals[11]. After correcting for in situ ^{10}Be contamination in Table Mountain samples, ref. 11 suggested using the mild leaching method (0.5 M HCl for 24 h at room temperature + 1 M hydroxylamine hydrochloride for 4 h in an 80 °C ultrasonic bath) of ref. 55. This leaching protocol has been shown to fully remove $^{10}Be_{met}$ and to release minimal in situ ^{10}Be[55].

To test the possible contamination from the aggressive leaching method, five Table Mountain (TM01) samples were duplicated using the mild leaching method. The $^{10}Be_{met}$ concentrations obtained using the mild leaching method were 1.64 times higher than the values obtained using the aggressive method[17] (Extended Data Fig. 3). Therefore, the concerns raised by ref. 11 about aggressive leaching and possible contamination from in situ ^{10}Be, which would have increased the measured $^{10}Be_{met}$ concentrations, were not applicable. The discrepancy found from the method of testing could be due to a combination of two main causes: (1) the leaching process and/or (2) the AMS measurement and sample calibration. The Table Mountain samples were originally analysed at the AMS facility at GNS Science and calibrated with the National Institute of Standards and Technology standard SRM 4325 (refs. 17,59,64). The different mass spectrometers used for each study along with natural variance could explain 10% difference at most[65]. Therefore, the larger (64%) difference requires another explanation. The aggressive HCl leach did not include a step to leach the $Be_{x\text{-}ox}$, of which ref. 55 calculated that 20 to 45% of the total $^{10}Be_{met}$ was located in this fraction. It is still unclear why higher concentrations were measured using the mild leach, but we hypothesize that the $Be_{x\text{-}ox}$ was not fully extracted by the aggressive HCl leach. HCl dissolves the most labile soil beryllium phases (poorly crystalline beryllium oxides). More-complex beryllium oxides need to be leached by reductive dissolution at acidic pH, which also prevents re-precipitation. This could therefore explain how the original Table Mountain samples had lower concentrations of $^{10}Be_{met}$. However, the risks of contamination using the aggressive method may not fully be ruled out, and to limit uncertainty, using the method of ref. 55 for all subsequent $^{10}Be_{met}$ leaching is recommended. Although the discrepancy in method needs further research, considering the offsets were consistent through all samples because

the leaches came from the same parent material and were within the same grain-size range, the offset was applied as a correction factor to all Table Mountain samples (Extended Data Fig. 3).

Closure ages using palaeosurface concentrations of $^{10}Be_{met}$

Here we use the two Miocene-age [$^{10}Be_{met}$] profiles to solve for one common variable: closure age (the time when $^{10}Be_{met}$ stopped infiltrating the ground and was sealed off in the sediment profile; Fig. 4b). The $^{10}Be_{met}$ flux that reaches a surface consists of two components: the meteoric flux (wet and dry deposition) and the aeolian flux, with the latter being a dominant mechanism in the MDV[11,16,17]. The regional proximity and the similar climatic and wind conditions of Friis Hills and Table Mountain allow two important assumptions to calculate closure ages of the soil profiles: (1) the flux of $^{10}Be_{met}$ is comparable at both sites and (2) $^{10}Be_{met}$ stopped migrating in the soil profiles at the same time (the closure ages are synchronous). Although the sites are separated by more than 500 m elevation, modern MAATs differ by <3 °C (−22.5 °C at Friis Hills[66] and −25 °C at Table Mountain[33]), making the sites sensitive to the same large-scale climatic shifts. These assumptions allow us to compare erosion rates at the two different sites. Dickinson et al. established that time since closure ages (yr) could be calculated using [$^{10}Be_{met}$] of the palaeosurface[17]:

$$t = \frac{-\ln \frac{N_{palaeo}}{N_{modern}}}{\lambda}. \quad (2)$$

where N_{palaeo} is the palaeosurface concentration of $^{10}Be_{met}$ (atoms g^{-1}) and N_{modern} is the modern surface concentration of $^{10}Be_{met}$ (atoms g^{-1}). The value of N_{palaeo} can be projected by fitting an exponential equation:

$$N_{palaeo} = ae^{bE} \quad (3)$$

where a and b are regression constants and E is a length measurement (multiplied by time) of the erosion rate ε described by the following equation:

$$\epsilon = \frac{Q}{N_{modern}} \quad (4)$$

where Q is the local flux of $^{10}Be_{met}$ (atoms cm^{-2} y^{-1}), ρ is the soil density (g cm^{-3}) and N_{modern} is the $^{10}Be_{met}$ concentration at the surface (atoms g^{-1}). By assuming that the closure age (t) was the same at each site (TM and FH), then:

$$\frac{N_{palaeoFH}}{N_{modernFH}} = \frac{N_{palaeoTM}}{N_{modernTM}} \quad (5)$$

In addition, by assuming that Q is the same for both sites and that erosion is lock stepped, and by reorganizing all variables[17]:

$$E_{TM=} \frac{_{FH}N_{modernFH}}{_{TM}N_{modernTM}} E_{FH} \quad (6)$$

and

$$E_{FH} = \frac{\ln \frac{a_{FH}N_{modernTM}}{a_{TM}N_{modernFH}}}{b_{FH} - b_{TM}\frac{_{FH}N_{modernFH}}{_{TM}N_{modernTM}}} \quad (7)$$

E_{FH} and E_{TM} can then be used to calculate erosion-corrected lower closure age using equations (2) and (3).

Assuming synchronous closure ages in the near surface, $^{10}Be_{met}$ concentrations yielded erosion rates of 0.011 m Myr^{-1} for TM01-97 (E_{TM}) and 0.095 m Myr^{-1} for FHDP2C (E_{FH}; Table 1). These results are within regolith erosion rates in the MDV (0.01 and 3.0 m Myr^{-1})[16,17,67]. This suggests that the erosion correction required for modelling closure ages is realistic. The closure age for the upper group at Friis Hills and Table Mountain calculated from the erosion-corrected N_{palaeo} was 6.0 ± 0.5 Myr. The uncertainty was derived from the $^{10}Be_{met}$ error (Extended Data Table 1) and the error of the fit parameters a and b (equation (3)) and propagated through our calculations for the closure age. Since the lower groups followed a linear regression where $b = 0$ and the near-surface profiles overprinted the intermediate profiles, fitting an exponential equation to solve for N_{palaeo} was not possible for the lower groups. The most realistic way to estimate N_{palaeo} for the lower groups was to use the b value from the upper groups and the same lock-stepped erosion rates. Closure age was then approximated using equation (2), which assumes that N_{modern} has not changed since closure. However, the closure age would increase if more $^{10}Be_{met}$ was retained at the surface, had the climate been wetter in the past[68]. On the basis of the $\delta^{13}C$ signal of C3 plants (−25.5 ± 0.7‰ Vienna PeeDee Belemnite (VPDB)), mean annual precipitation of 150–450 mm yr^{-1} was estimated for Friis Hills during the mid-Miocene[69]. Using a modern analogue for surface $^{10}Be_{met}$ concentration with similar $\delta^{13}C$ values, such as Northern Sweden ($\delta^{13}C$ = −26.0‰ VPDB, $^{10}Be_{met} = 2.0 \times 10^8$ atoms g^{-1})[70–74], $^{10}Be_{met}$ surface concentrations could have been approximately four times higher. The decay required to obtain current $^{10}Be_{met}$ concentrations can be modelled using the maximum N_{modern}. This age represents an estimate of maximum closure age for the lower group (assuming lock-stepped erosion). A maximum closure age of ~12.0 Ma for FHDP2C and ~16.0 Ma for TM01-97 for the lower section of the cores was calculated. However, these ages need to be treated with caution as they represent only a broad estimate of time required for $^{10}Be_{met}$ concentrations in the 10^8 atoms g^{-1} range to decay to 10^5 atoms g^{-1}. Similarly, using the average $^{10}Be_{met}$ concentration for the deep samples as N_{palaeo}, the closure age at 40 m depth at Friis Hills was ~14.0 Ma, the same as the age of the sediment.

Data availability

The dataset is available in Extended Data Tables 1–3.

Code availability

The latest version of the PERICLIMv1.0 model is available as an R package from https://github.com/tomasuxa/PERICLIMv1.0 (last accessed 30 January 2022).

References

55. Wittmann, H. et al. The dependence of meteoric ^{10}Be concentrations on particle size in Amazon River bed sediment and the extraction of reactive $^{10}Be/^{9}Be$ ratios. *Chem. Geol.* **318**, 126–138 (2012).
56. Tessier, A., Campbell, P. G. & Bisson, M. Sequential extraction procedure for the speciation of particulate trace metals. *Anal. Chem.* **51**, 844–851 (1979).
57. Bourles, D., Klinkhammer, G., Campbell, A., Brown, E. & Edmond, J. Beryllium in marine pore waters: geochemical and geochronological implications. *Nature* **341**, 731–733 (1989).
58. Guelke-Stelling, M. & von Blanckenburg, F. Fe isotope fractionation caused by translocation of iron during growth of bean and oat as models of strategy I and II plants. *Plant Soil* **352**, 217–231 (2012).
59. Nishiizumi, K. et al. Absolute calibration of ^{10}Be AMS standards. *Nucl. Instrum. Methods Phys. Res. B* **258**, 403–413 (2007).
60. Graham, I. et al. Dating Antarctic soils using atmosphere-derived ^{10}Be and nitrate. in *Antarctica at the Close of a Millennium* (eds Gamble, S. et al.) 429–436 (Royal Society of New Zealand, Wellington, 2002).
61. Schiller, M. *Testing the Antiquity of McMurdo Dry Valley Soil Surfaces with Atmospheric ^{10}Be*. MSc thesis, Victoria Univ. Wellington (2007).
62. Graham, I., Ditchburn, R. & Whitehead, N. Be isotope analysis of a 0–500 ka loess–paleosol sequence from Rangitatau East, New Zealand. *Quat. Int.* **76**, 29–42 (2001).

63. Ditchburn, R. G. & Graham, I. *Preparation Procedures for the ^{10}Be Analysis of Marine Deposits* Report No. INIS 26 (Institute of Geological and Nuclear Sciences, 2002).
64. Zondervan, A., Poletti, M., Purcell, C. R. & Sparks, R. J. Accelerator and beamline upgrades at the AMS facility of GNS Science, New Zealand. *Nucl. Instrum. Methods Phys. Res. B* **259**, 47–49 (2007).
65. Jull, A. T., Scott, E. M. & Bierman, P. The CRONUS-Earth inter-comparison for cosmogenic isotope analysis. *Quat. Geochronol.* **26**, 3–10 (2015).
66. Obryk, M. K., Doran, P. T., Fountain, A. G., Myers, M. & McKay, C. P. Climate from the McMurdo Dry Valleys, Antarctica, 1986–2017: surface air temperature trends and redefined summer season. *J. Geophys. Res. Atmos.* **125**, e2019JD032180 (2020).
67. Morgan, D. J., Putkonen, J., Balco, G. & Stone, J. Degradation of glacial deposits quantified with cosmogenic nuclides, Quartermain Mountains, Antarctica. *Earth Surf. Process. Landf.* **36**, 217–228 (2011).
68. Field, C. V., Schmidt, G. A., Koch, D. & Salyk, C. Modeling production and climate-related impacts on ^{10}Be concentration in ice cores. *J. Geophys. Res. Atmos.* **111**, D15107 (2006).
69. Kohn, M. J. Carbon isotope compositions of terrestrial C3 plants as indicators of (paleo) ecology and (paleo) climate. *Proc. Natl Acad. Sci. USA* **107**, 19691–19695 (2010).
70. Ebert, K., Willenbring, J., Norton, K. P., Hall, A. & Hättestrand, C. Meteoric ^{10}Be concentrations from saprolite and till in northern Sweden: implications for glacial erosion and age. *Quat. Geochronol.* **12**, 11–22 (2012).
71. Jelinski, N. A. *Problems of Physical Movement in Soil Genesis: Application of Meteoric Beryllium-10 as a Component of Multi-tracer Analysis*. PhD thesis, Univ. Minnesota (2014).
72. Andersland, O. & Anderson, D. *Geotechnical Engineering for Cold Regions* (McGraw-Hill, 1978).
73. Cannone, N. & Guglielmin, M. Influence of vegetation on the ground thermal regime in continental Antarctica. *Geoderma* **151**, 215–223 (2009).
74. Hrbáček, F., Nývlt, D. & Láska, K. Active layer thermal dynamics at two lithologically different sites on James Ross Island, Eastern Antarctic Peninsula. *Catena* **149**, 592–602 (2017).
75. Streletskiy, D. A. et al. CALM north summary data table. *The George Washington University* https://www2.gwu.edu/~calm/data/north.htm (2022).

Acknowledgements

The Friis Hills Drilling Project (austral summer 2016–2017) was funded by the New Zealand Ministry of Business, Innovation and Employment through the Past Antarctic Science Programme (C05X1001) and the Antarctic Science Platform (ANTA1801) to R.L. and T.N. The sampling at University Valley was funded by a NASA-ASTEP grant. Fieldwork at Friis Hills and Table Mountain was made possible with the logistical support of Antarctica New Zealand. We thank A. Pyne, R. Pyne, H. Chorley and Webster Drilling for retrieving the cores at Friis Hills. A special thank you to N. Bertler for allowing us to use the GNS Ice Core Facility to store and sample the permafrost cores. Laboratory work was made possible with the help of the technical staff at the Cosmogenic Nuclide Laboratory at the Victoria University of Wellington (L. Ashworth) and the Laboratory of Ion Beam Physics at ETH, Zürich (P. Gautschi). AMS analysis was in part funded by an Antarctic Science International Ltd Bursary to M.V.

Author contributions

M.V., W.D., K.N. and D.L. designed this project and contributed to data analysis/interpretation and writing the manuscript. C.T.-L. analysed the preliminary samples from Friis Hills (FA, C1 and C2) and University Valley. M.C. ran the $^{10}Be_{met}$ samples, including AMS data reduction. R.L. and T.N. developed the Friis Hills Drilling Project. All authors edited the whole manuscript.

Competing interests

The authors declare no competing interests.

Additional information

Extended data is available for this paper at https://doi.org/10.1038/s41561-023-01193-4.

Supplementary information The online version contains supplementary material available at https://doi.org/10.1038/s41561-023-01193-4.

Correspondence and requests for materials should be addressed to Marjolaine Verret.

Peer review information *Nature Geoscience* thanks Paul Bierman and the other, anonymous, reviewer(s) for their contribution to the peer review of this work. Primary Handling Editor: James Super, in collaboration with the *Nature Geoscience* team.

https://doi.org/10.1038/s41561-023-01193-4

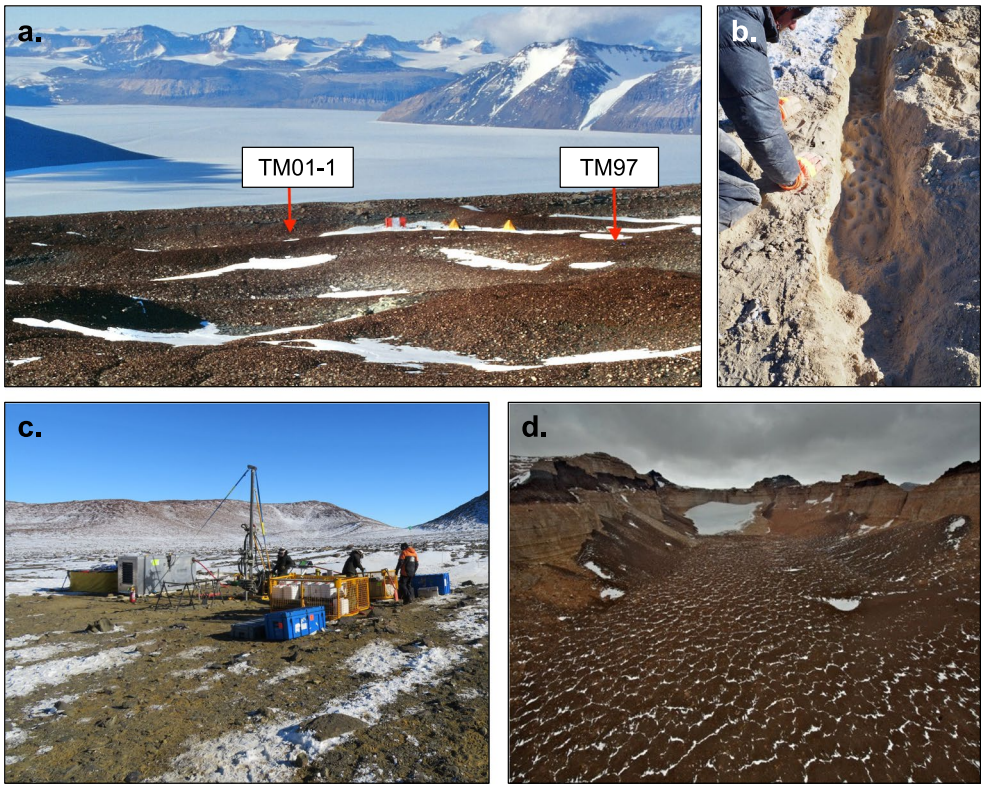

Extended Data Fig. 1 | Photos of the location sites. Photos of the location sites: a. Table Mountain core sites (TM01-1 and TM97) on desert pavement lying above Sirius Group sediments with Ferrar Glacier in the backdrop (photo credit: Warren Dickinson), b. ice table excavated at 30 cm depth at Friis Hills (photo credit: Richard Levy), c. drilling rig retrieving cores during the 2016-2017 Friis Hills Drilling Project (photo credit: Richard Levy) and, d. University Valley site with polygonal ground (photo credit: Denis Lacelle).

https://doi.org/10.1038/s41561-023-01193-4

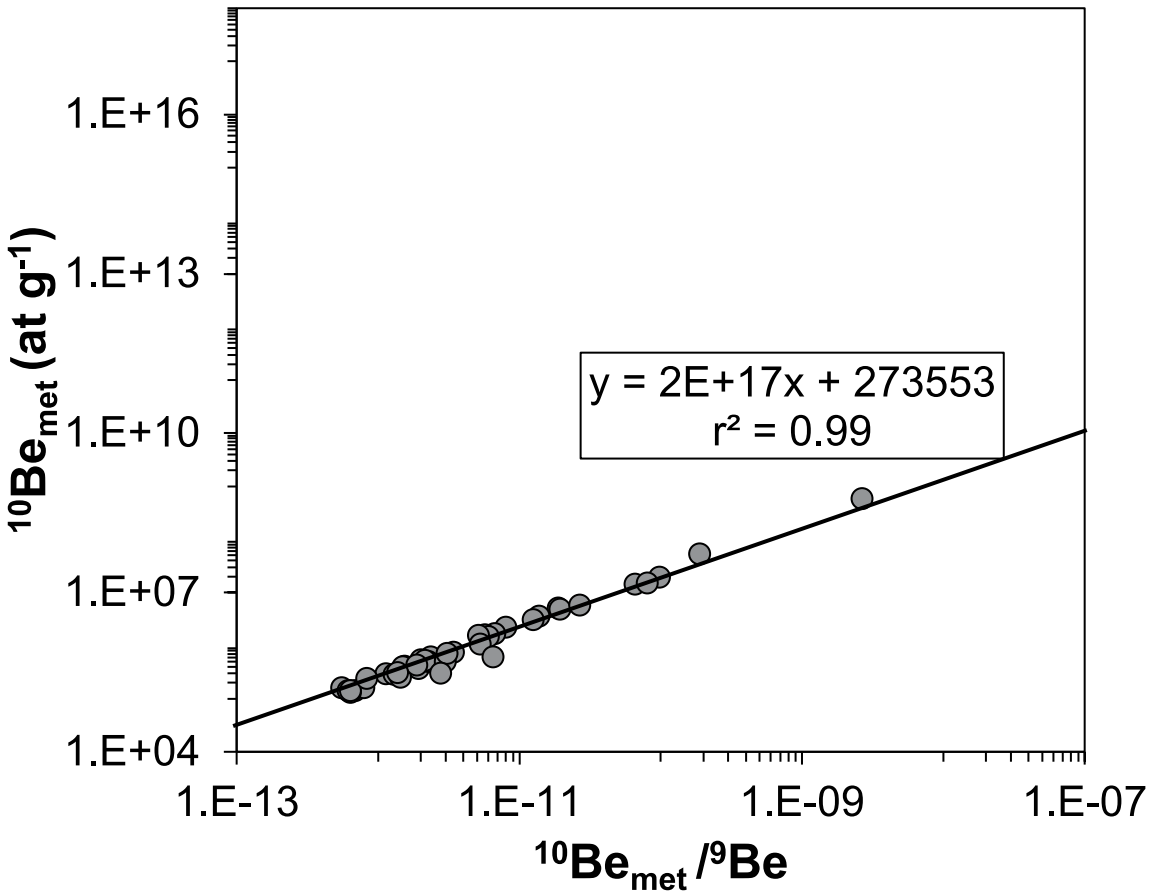

Extended Data Fig. 2 | $^{10}Be_{met}$ and $^{10}Be_{met}/^{9}Be$ biplot. Note: here, ^{9}Be is measured independently on a MP-AES.

https://doi.org/10.1038/s41561-023-01193-4

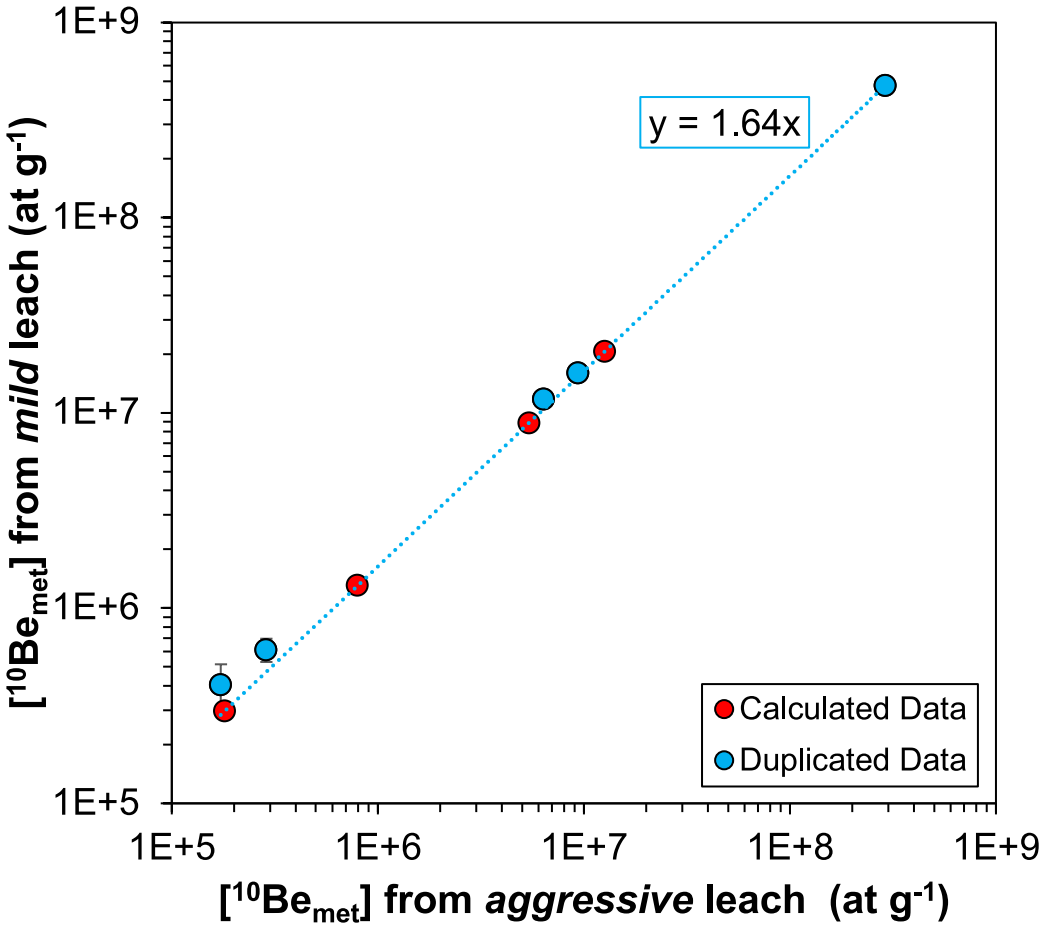

Extended Data Fig. 3 | Duplicate samples at Table Mountain showing $^{10}Be_{met}$ concentrations measured by aggressive and mild leaching methods. Duplicate samples at Table Mountain showing $^{10}Be_{met}$ concentrations measured by aggressive[17] and mild leaching methods. Dataset in red offset using the duplicate function.

https://doi.org/10.1038/s41561-023-01193-4

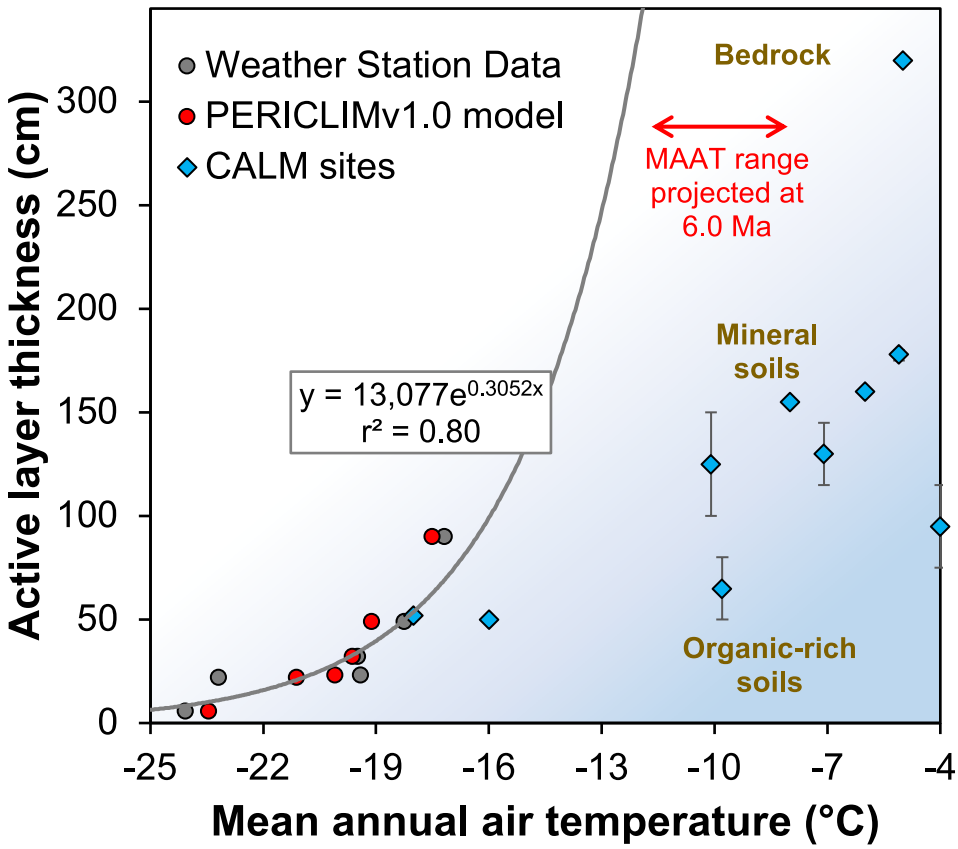

Extended Data Fig. 4 | Comparison between mean annual air temperature and active layer measurements at different sites in the MDV and values predicted by the PERICLIMv1.0. model. Comparison between mean annual air temperature and active layer measurements at different sites in the MDV[35] and values predicted by the PERICLIMv1.0. model[36]. Data is compared to selected median values of Circumpolar Active Layer Monitoring (CALM) sites for the 1990–2011 period (n = 22 with data gaps)[75]. Error bars represent the range of active layer measured during the studied period.

https://doi.org/10.1038/s41561-023-01193-4

Extended Data Table 1 | Measured and calculated values of $^{10}Be_{met}$ in preliminary sites at Friis Hills

Sample ID	Depth (cm)	$^{10}Be/^{9}Be$ (10^{-12})	Error (%)	$^{10}Be_{met}$ (at g^{-1})	$^{10}Be_{met}$ Error (at g^{-1})
FRIIS HILLS (FA; 161°34'39"E, 77°45'00"S)					
FA-0	0	2.027	2.4	5.92E+07	1.40E+06
FA-5	5	0.199	7.5	5.85E+06	4.41E+05
FA-10	10	0.093	6.9	2.71E+06	1.87E+05
FA-30	30	0.093	9.9	2.70E+06	2.67E+05
FA-60	60	0.041	15.3	1.19E+06	1.83E+05
FRIIS HILLS (C2; 161°27'38"E, 77°45'13"S)					
C2-0	0	7.344	2.0	2.15E+08	4.30E+06
C2-5	5	0.096	11.3	2.83E+06	3.21E+05
C2-10	10	0.114	10.0	3.33E+06	3.32E+05
C2-32	32	0.054	12.6	1.58E+06	1.98E+05
C2-59	59	0.051	20.6	1.50E+06	3.09E+05
FRIIS HILLS (C1; 161°26'49"E, 77°45'15"S)					
C1-0	0	0.049	13.4	1.45E+06	1.95E+05
C1-17	17	0.030	27.7	8.85E+05	2.45E+05
LAB BLANK					
Blank	N.A.	0.003	57.7	N.A.	N.A.

These samples were leached using the *mild* method and measured on the 500 kV AMS (TANDY, ETH Zürich, 2018).

https://doi.org/10.1038/s41561-023-01193-4

Extended Data Table 2 | Measured and calculated values of $^{10}Be_{met}$ at University Valley

Sample ID	Depth (cm)	$^{10}Be/^{9}Be$ (10^{-12})	Error (%)	$^{10}Be_{met}$ (at g^{-1})	$^{10}Be_{met}$ Error (at g^{-1})
UNIVERSITY VALLEY (P1; 160°42'07"E, 77°51'54"S)					
P1 0-5	2.5	4.870	1.8	9.13E+08	1.64E+07
P1 15-20	17.5	1.980	1.8	3.65E+08	6.58E+06
P1 30	30	1.500	1.8	3.08E+08	5.69E+06
P1 43	43	1.300	2.0	2.49E+08	5.01E+06
P1 53	53	1.490	2.0	2.89E+08	5.85E+06
UNIVERSITY VALLEY (P2; 160°42'32"E, 77°51'32"S)					
P2 0-5	2.5	11.60	1.8	2.17E+09	3.91E+07
P2 20	20	0.330	3.0	6.25E+07	1.88E+06
P2 20-25	22.5	0.741	2.0	1.37E+08	2.71E+06
P2 34	34	0.609	1.8	1.13E+08	2.03E+06
P2 42	42	0.752	1.8	1.43E+08	2.57E+06
UNIVERSITY VALLEY (P8; 160°43'34"E, 77°51'54"S)					
P8 2	2	2.70	1.8	4.99E+08	8.99E+06
P8 16	16	0.121	2.5	2.45E+07	6.23E+05
P8 26	26	0.121	2.7	2.23E+07	6.17E+05
LAB BLANK					
Blank	N.A.	0.001	1.7	N.A.	N.A.

These samples were leached using the mild method and measured on the 500 kV AMS (TANDY, ETH Zürich, 2017).

https://doi.org/10.1038/s41561-023-01193-4

Extended Data Table 3 | Measured and calculated values of $^{10}Be_{met}$ at Friis Hills and Table Mountain

Sample ID	Depth (cm)	$^{10}Be/^{9}Be$ (10^{-12})	Error (%)	$^{10}Be_{met}$ (at g^{-1})	$^{10}Be_{met}$ Error (at g^{-1})
FRIIS HILLS (FHDP2C; 161°27'21"E, 77°45'17"S)					
2-C0-1[A]	1	2.294	1.5	4.37E+07	8.07E+05
2-C0-2[A]	5	0.200	3.5	4.11E+06	1.76E+05
2-C0-3[A]	10	0.209	3.6	3.94E+06	1.76E+05
2-C0-4[A]	15	0.157	3.9	2.88E+06	1.41E+05
2-C0-5[A]	20	0.258	3.3	4.67E+06	1.90E+05
2C-C1-2[A]	38	0.125	4.8	2.49E+06	1.50E+05
2C-C1-10[A]	59.5	0.085	6.1	1.82E+06	1.38E+05
2C-C1-18[A]	78	0.070	5.6	1.38E+06	9.71E+04
2C-C1-22[A]	97	0.062	7.8	1.30E+06	1.27E+05
2C-C1-29[A]	116.5	0.067	5.9	1.21E+06	8.98E+04
2C-C2-8[B]	135.5	0.052	8.1	1.25E+06	1.27E+05
2C-C2-26[B]	189.5	0.024	15.9	4.96E+05	1.02E+05
2C-C3-3[B]	246	0.020	12.7	2.98E+05	5.09E+04
2C-C3-16[B]	286.5	0.019	11.5	4.35E+05	6.54E+04
2C-C4-9[B]	336.5	0.023	14.4	4.02E+05	7.63E+04
2C-C4-20[B]	364.5	0.011	15.8	2.33E+05	5.05E+04
2C-C5-2[B]	459	0.024	13.4	4.25E+05	7.45E+04
2C-C5-11[B]	490	0.017	12.1	3.29E+05	5.34E+04
2C-C5-20[B]	510.5	0.016	13.0	3.20E+05	5.57E+04
FRIIS HILLS (FHDP3A; 161°26'46"E, 77°45'09"S)					
3A-C27-1[B]	3717.5	0.014	13.7	2.28E+05	4.34E+04
3A-C27-2[B]	3736.5	0.013	15.3	2.03E+05	4.36E+04
3A-C28-1[B]	3785.5	0.007	23.8	1.28E+05	4.54E+04
3A-C33-1[C]	4265.5	0.008	16.5	1.11E+05	2.85E+04
3A-C33-2[C]	4307	0.009	15.1	1.25E+05	2.88E+04
3A-C33-3[C]	4333.75	0.008	18.1	1.03E+05	2.94E+04
3A-C33-4[C]	4337	0.021	14.8	3.45E+05	6.78E+04
3A-C33-5[C]	4341.5	0.007	22.4	1.12E+05	3.85E+04
3A-C33-6[C]	4344.5	0.008	18.3	1.11E+05	3.14E+04
3A-C34-1[C]	4411.5	0.010	16.8	1.92E+05	4.54E+04
TABLE MOUNTAIN (TM01; 77°57'36"S, 161°57'15"E/TM97)					
TM01-S1[C]*	3	22.667	1.5	4.75E+08	8.77E+06
TM01-S2[D]*	27	0.856	2.3	1.60E+07	4.49E+05
TM01-9[D]*	140.5	0.545	2.9	1.18E+07	4.24E+05
TM01-25[D]*	339	0.033	10.7	6.13E+05	8.41E+04
TM01-37[D]*	463.5	0.023	20.9	4.06E+05	1.11E+05
TM01-42[D]	525.5	0.041	13.0	8.62E+05	1.42E+05
TM01-44[D]	575	0.028	15.2	5.82E+05	1.14E+05
TM01-48[D]	607	0.014	15.6	2.45E+05	5.25E+04
TM97-7B-1[D]	745	0.030	16.4	4.98E+05	1.06E+05
TM97-7B-2[D]	885	0.015	14.4	2.42E+05	4.81E+04
LAB BLANKS					
Blank 1[A]	N.A.	0.008	18.2	N.A.	N.A.
Blank 2[B]	N.A.	0.004	30.1	N.A.	N.A.
Blank 3[C]	N.A.	0.001	53.9	N.A.	N.A.
Blank 4[D]	N.A.	0.003	37.8	N.A.	N.A.

These samples were measured on the 300 kV AMS (MILEA, ETH Zürich, 2019). *Samples marked with a * were rerun for the method of testing described in the Methods section and shown in* Extended Data Fig. 3. (Note: [A-D] indicates which blank is associated to which sample).

https://doi.org/10.1038/s41561-023-01193-4

Extended Data Table 4 | Values of parameters used in PERICLIMv1.0 model

Input Parameters	Values
Thaw depth [m]	2.74 – 3.45
Thawed ground thermal conductivity [W $m^{-1}K^{-1}$]	2.5[a]
Volumetric ground moisture content [-]	0.3
Thawing n-factor [-]	~3.0[b]
Annual air temperature amplitude [°C]	37[c]
Period of air temperature oscillations [d]	365

[a] retrieved from [72] for sandy soils

[b] determined from wet bare Antarctic ground [73,74]

[c] retrieved from [38]